Structural relationships in and around the Rheasilvia basin on Vesta

Hiu Ching Jupiter Cheng[1] and Christian Klimczak[1]

[1]Center for Planetary Tectonics, Department of Geology, University of Georgia, Athens, GA 30602, USA

Abstract

The Rheasilvia basin is an impact structure occupying most of Vesta's southern hemisphere. Divalia Fossae, a set of circum-equatorial troughs, were previously proposed to be concentric around the basin, which is widely regarded as evidence that the Rheasilvia impact directly caused the formation of the troughs. Here, we produce a structural map of Rheasilvia that allows for geologic interpretations and quantitative analyses of structure orientations and densities. We mapped basin-bounding scarps, scarps within the basin, ridges, and undefined lineaments. Scarps abound near the basin rim, with ridges being densely located on the basin floor near the central mound, forming a spiral pattern. This pattern is well-preserved on the basin floor except in the area superposing the older Veneneia basin, indicating that pre-existing Veneneia structures substantially influenced those of Rheasilvia. This implies that the lithosphere must have remained highly shattered after the Veneneia impact until Rheasilvia was emplaced. The Divalia Fossae cross-cut the Rheasilvia basin, and reanalysis of the geometric relationship between both landforms reveals that the troughs are not concentric around the basin center. These results are inconsistent with the previous hypothesis of trough formation and require a reconsideration of Vesta's tectonic history.

1. Introduction

1.1. Geology of the Rheasilvia Basin

The existence of a major impact basin on Asteroid 4 Vesta, hereon referred to as Vesta, was first hypothesized when Hubble Space Telescope observations revealed a large depression in the south polar region of the asteroid (Thomas et al., 1997). The Dawn mission to Vesta (Russell and Raymond, 2011) revealed that the basin is 450 km in diameter, which is ~85% of the mean diameter of the asteroid, and that it occupies a large portion of the southern hemisphere. The impact that formed the basin is thought to be the youngest global-scale impact on Vesta (Schenk et al., 2012), and it likely excavated sufficient crustal material to have created the Vestoid asteroid family (Marzari et al., 1996; Asphaug, 1997) and the howardite–eucrite–diogenite (HED) meteorites (McCord et al., 1970; Drake and Consolmagno, 1977).

The Framing Camera (FC; Sierks et al., 2011) aboard the Dawn spacecraft captured high-resolution images of the Rheasilvia basin (Roatsch et al., 2015), allowing the construction of a detailed digital terrain model (DTM; Figure 1; Preusker et al., 2016). The Rheasilvia basin is roughly hexagonal and outlined by discontinuous scarps (Figure 1; Schenk et al., 2012), with the most prominent one named Matronalia Rupes (Figure 1). No large melt sheet associated with the impact is observed, and its absence is interpreted to indicate a slow impactor (O'Brian and Sykers, 2011). Spacecraft observations also revealed a second large basin, Veneneia, that is partly superposed by the Rheasilvia basin. Veneneia is inferred to have a diameter of ~421 km (Figure 1; Jaumann et al., 2012; Marchi et al., 2012; Schenk et al., 2012). The basin rim of Rheasilvia that superposes the Veneneia depression has a lower elevation when compared with those portions of the rim that fall outside this depression (Figure 1). This asymmetry was previously interpreted to be caused either by the pre-existing Veneneia topography (Collins et al., 2008) or by an oblique impact (Poelchau and Kenkmann, 2008).

<insert Figure 1>

Yingst et al. (2014) mapped terrains and structures of the Rheasilvia basin as part of the geological mapping effort of Vesta. The basin has a large central mound, a broad sloping basin floor with ridge-and-groove terrain, and mass-wasting materials. The irregular central mound (Figure 1) is bisected by structures aligned with the larger structural trend of the basin floor. The basin floor has curvilinear ridges, grooves, and inward-facing scarps of kilometers to tens of kilometers long and a few kilometers high. These structures form two pronounced trends with one sub-radial from the mound and another parallel to basin-bounding scarps, generating a pervasive clockwise spiral pattern across the basin floor (Figure 1; Schenk et al., 2012; Yingst et al., 2014).

Numerical modeling (Jutzi et al., 2013) and the prediction of mass motion related to the Rheasilvia impact on a fast-spinning asteroid (Otto et al., 2016) support that these structures are remnants of mass wasting that occurred during the original modification with their orientations influenced by the Coriolis effect (Schenk et al., 2012; Otto et al., 2013; Jutzi et al., 2013). Mass-wasting materials were deposited along the bases of steep slopes and basin-bounding scarps, indicating the mobility of the regolith (Jaumann et al., 2012; Pieters et al., 2012). Several types of mass-wasting structures are identified within the Rheasilvia basin, including flow-like patterns, creep-like mounds (which are elongated features with a straight or slightly curved shape), rotational slumping, landslides, and curved ridges (Otto et al., 2013).

The geomorphology of the Rheasilvia basin is unlike those of large multi-ring impact structures on other terrestrial bodies, such as the Moon and Mercury (Melosh, 1989), but it is like large (complex) craters on low-gravity bodies with deep depressions and broad central mounds (Schenk et al., 2012). The spiral deformation pattern within the Rheasilvia basin is unique among large impact structures throughout the solar system in its size and preservation. Although these structures have been mapped at a large scale or locally in multiple works (e.g., Otto et al, 2013; Krohn et al., 2014; Yingst et al., 2014), a detailed structural map has not been constructed for the entire basin using a set of clearly defined and consistently applied mapping criteria. The basin is outlined by stratigraphic units in the geologic map from Yingst et al. (2014), but the rim and its center have yet to be defined by structural mapping and geometric analysis.

1.2. Basin relationship with Divalia Fossae

Dawn images also revealed the presence of two sets of large-scale troughs named Divalia and Saturnalia Fossae. The Divalia Fossae encircle about two-thirds of the asteroid at the equator, and their width ranges from several 100s of meters to 20.5 km. The Saturnalia Fossae are oriented northwest–southeast, and differ in orientation from the Divalia Fossae by approximately 30°. They are exposed only in the northern hemisphere, and their southern extent is truncated by the Divalia Fossae. The poles of vertical planes defined along the Divalia and Saturnalia Fossae cluster near the centers of Rheasilvia and Veneneia impact basins, respectively, which is widely regarded as a genetic link between the troughs and basins (Jaumann et al., 2012; Scully et al., 2014; Schäfer et al., 2014). In particular, the impact that led to the emplacement of the Rheasilvia basin is proposed to have occurred at the south pole with no later reorientation of the asteroid (Karimi and Dombard, 2016) directly triggering the formation of the Divalia Fossae at the equator (Bowling et al., 2014; Stickle et al., 2015).

Numerical experiments show that stresses from the impact shock wave were localized in the equatorial region and caused fracturing (Bowling et al., 2014; Stickle et al., 2015). The underlying fracturing mode that is responsible for the formation of the troughs was assumed to be normal faulting (Buczkowski et al., 2012), but our recent research points to an opening-mode or mixed-mode fracture origin of the troughs (Cheng and Klimczak, 2022). The scenario described here for the formation of the Divalia Fossae by the impact that formed the Rheasilvia basin is also invoked for the Saturnalia Fossa and Veneneia impact.

The geographic relationship of the poles of vertical planes through the troughs clustering near the center of the basin is the only observation that suggests the formation of the Divalia and Saturnalia Fossae were caused by the impacts that led to the emplacements of the Rheasilvia and Veneneia basins. The implication that arises from this scenario is that the troughs and basins must have formed simultaneously, specifically that the Divalia Fossae must have formed coevally with the Rheasilvia impact and the Saturnalia Fossae with the Veneneia impact. No cross-cutting relationships between the Divalia Fossae and Rheasilvia basin (and Saturnalia Fossae and Veneneia basin) that could provide relative ages have been documented, such that age relationships rely only on comparisons of crater frequencies on the two landform types (Cheng et al., 2021). Although the reported crater frequencies permit their simultaneous formation, large uncertainties allow for the Divalia Fossae to have formed well before or after the emplacement of the Rheasilvia basin (Cheng et al., 2021).

Moreover, stratigraphic relationships of the Rheasilvia basin with the geological units and structures in Vesta's northern hemisphere are mostly inferred from the assumed simultaneous basin formation with the Divalia Fossae. For example, the Divalia Fossae crosscut the Saturnalia Fossae and cratered highland units, which led to the inference that the Rheasilvia basin postdates these units in the global stratigraphy (Schäfer et al., 2014; Williams et al., 2014; Yingst et al., 2014). Any additional findings on the relative timing of troughs and basins, especially the Rheasilvia basin and Divalia Fossae will help better constrain the geologic history of Vesta.

The relationship between the Rheasilvia basin and Divalia Fossae plays an important role in determining the tectonic and, more broadly, the geological evolution of Vesta, as well as large impact structures on small bodies in general. That large impacts cause geologic activity far from the site of impact is not surprising, as antipodal focusing of seismic waves and ejecta is widely hypothesized to trigger volcanism or tectonics (e.g., Schultz and Gault, 1975; Williams and Greely, 1994; Schultz and Crawford, 2011; Meschede et al., 2011). On Vesta, ancient cratered highlands and small-scale linear depressions are present near the north pole at the antipode of the Rheasilvia impact (Blewett et al., 2014), but large-scale troughs or other tectonic or volcanic phenomena are absent at the antipode (Bowling et al., 2013). “Hilly and lineated terrains” that are found at the antipodes of large basins on the Moon and Mercury (e.g., Schultz and Gault, 1975; Murray et al., 1974; Melosh and McKinnon, 1988) are also absent at the Rheasilvia or Veneneia antipodes.

Numerical studies reveal that troughs, grooves, or other lineaments could be formed by a large impact on small bodies (Asphaug et al., 1996; Benz and Asphaug, 1994), and observations on asteroid Ida corroborating this finding. However, grooves and lineaments on Ida occur in the antipodal region of a large impact structure. Prominent grooves not at the antipode of impact structures, such as those on Mars’ moon Phobos, are unlikely to have an impact origin (Wilson and Head, 2015). That the Divalia Fossae are tied to an impact structure but are not localized at the antipodal region but instead at 90° from the impact distinguishes them from the Moon, Mercury, and other small bodies, and leaves open the question of why they are localized in the equatorial region of Vesta.

1.3. Goals of the study

Basin-bounding and intra-basin structures of the Rheasilvia basin have yet to be systematically and consistently mapped and described in detail using Dawn-derived photogeological datasets. A detailed structural map that documents the distribution of different structure types is the basis for further analyses that assess cross-cutting relationships among intra-basin structures as well as structural orientations and patterns. Cross-cutting relationships, orientations, and patterns of structures may reveal the deformation that took place during or after the basin was emplaced. Determining the structural outline of the Rheasilvia basin allows us to recalculate the basin center and reassess its location with respect to the Divalia Fossae. This work aims to (1) produce a detailed structural map of the Rheasilvia basin using consistent and rigorous mapping criteria, (2) quantify the orientations and pattern of basin structures with length-weighted rose diagrams in regional bins, (3) analyze the density of each type of structures and their relationships within the basin, (4) assess the cross-cutting relationships among the intra-crater structures and with other structures, including impact craters and the Divalia Fossae, and (5) determine the geographic relationship of the Rheasilvia basin and the Divalia Fossae with our mapping. These results will contribute towards understanding the post-emplacement Rheasilvia basin and global tectonics on Vesta.

2. Methodology

2.1. Structural map production and quantitative analyses

We conducted structural mapping on the HAMO-based Dawn FC clear filter image mosaic that has an average resolution of 60 m/pixel (Roatsch et al., 2015). We complemented the image mosaic by calculating several hillshade maps with the shade function in the open-access USGS software ISIS3 from the ~70 m/pixel DTM (Figure 1; Preusker et al., 2016). Our mapping was further assisted with topographic profiles in *ESRI's ArcGIS software*. The topographic expression of a structure is distinctly shown when the structure is perpendicular to the source of illumination on the hillshade. To capture all basin structures, we computed four hillshades for different solar azimuths (Figure 2), including 56°E, 146°E, 124°W, and 34°W, with a fixed zenith of 45° for all hillshades.

<insert Figure 2>

These datasets were projected to a south-pole stereographic projection using a 255-km-diameter sphere model. We used the Claudia Double-Prime system (Li et al., 2012; WGCCRE., 2014), a coordinate system for Vesta adopted by the International Astronomical Union (IAU) Working Group on Cartographic Coordinates and Rotational Elements (WGCCRE) since 2014[1], which assigns a positive longitude of 146° to the Claudia crater. Literature prior to that (e.g., Roatsch et al., 2012; Russell et al., 2012) use the ''Claudia' system (the original coordinate system for Vesta), in which the longitude of Claudia crater is assigned as 0°.

Three types of basin structures were mapped based on their topographic expressions (Figure 3), specifically *scarps*, *ridges*, and *undefined lineaments*, which we define below. Basin

[1] https://www.iau.org/news/announcements/detail/ann14003/

structures were previously described as ridges, grooves, and scarps (see section 1.1. of this manuscript), with grooves being defined by the depressions between two ridges or two oppositely down-dipping scarps; thus, they are not included as a separate type of structure in this study. Apart from ridges and scarps, the surface texture of the basin is also defined by densely intersecting lineaments visible on the FC imagery, which have not been mapped before and are therefore included in our mapping.

Scarps are here defined as long and narrow linear structures that display a sharp topographic break. The scarp surface appears to be distinctively bright when facing the sun and is in the shade when facing away from the sun (Figures 3a,b). All scarps were mapped by placing a polyline along the top of the continuous sharp topographic break as shown in the topographic profile (Figure 3c) and presented using map symbols with the tick marks indicating the downslope direction (Figure 3d). We further designated the most prominent scarps that define the edge of the Rheasilvia basin as *basin-bounding scarps*. These scarps are meaningful for outlining the basin perimeter, and they help define the basin center.

<insert Figure 3>

Ridges are defined as long, narrow, positive-relief structures. The slope facing the illumination appears as a bright surface that gradually darkens as the slope becomes less steep near the crest with the opposite slope being in the shade or less illuminated (Figures 4a,b). Continuous ridge crests are identified (Figure 4c) and traced in the mapping (Figure 4d) using map symbols with a pair of arrows pointing away from one another indicating the downslope of the two sides of the ridge. *Undefined lineaments* are linear structures that are seen on the FC images (Figure 5a), but they are too fine to display any characteristic topographic properties in the hillshades or topographic profiles (Figures 5b,c). These structures were mapped entirely based on the FC imagery (Figure 5d).

<insert Figures 4 and 5>

All structures are mapped at a fixed map scale of 1:200,000 as polylines with regularly spaced vertices set to 1 km by using the streaming function of the ArcMap Editor to ensure equal and consistent sampling for further orientation and spatial density analyses in this work. The structural map is provided as supplementary shapefiles that can be viewed and edited in an ArcGIS environment.

2.2. Determination of the basin and troughs configurations

To determine the geographic relationship of the Divalia Fossae and the Rheasilvia basin, we need to determine the planes defined by the troughs and compare their poles with the previously calculated basin center. We used the dataset from Cheng and Klimczak (2022), which includes maps of all 19 trough segments of Divalia Fossae. The planes of these troughs and their poles were calculated using *Stereonet 11* (Allmendinger et al., 2013; Cardozo and Allmendinger, 2013). After that, we computed the ellipse of the 95% confidence interval for the locations of the poles in *Stereonet 11* and compared it with the two center points for the Rheasilvia basin, including our calculated center and the original one defined by Jaumann et al. (2012), who determined the center of the basin by fitting a perfect circle to the basin.

3. Rheasilvia basin structures

3.1. Structural map

We mapped 30 prominent basin-bounding scarps with a total length of 1311 km, 563 scarps within the basin with a total length of 8586 km, 494 ridges with a total length of 5814 km, and 4393 undefined lineaments with a total length of 29340 km (Figure 6). We included the floors and rims of those impact craters with diameters greater than 20 km that were listed in the crater catalogue in Liu et al. (2018) to provide a full picture of the structures of the basin floor and to investigate cross-cutting relationships between the craters and structures. We also included the troughs and their bounding scarps of the Divalia Fossae from Cheng and Klimczak (2022) in the structural map to explore the cross-cutting relationships of the troughs and basin.

<insert Figure 6>

The basin is asymmetrically hexagonal and outlined by basin bounding-scarps, consistent with previous study (Schenk et al., 2012). We calculated the geometric mean center of the basin based on the basin-bounding scarps and estimate it at 69.3°S and 95.5°E (Figure 6). Our calculated center somewhat differs from the basin center of 75°S and 87°E of Jaumann et al. (2012), who defined the center by fitting a perfect circle to the basin structure and did not account for the true basin shape. Both centers are located on the central mound of the Rheasilvia basin. We estimated the extent of the Veneneia basin that is superposed by the Rheasilvia basin as a circle using the three-point method in the *CraterTools plug-in* (Kneissl et al., 2011) by identifying three points along the preserved basin scarps. The resulting circular area has a ~420 km-diameter (Figures 1 and 6), consistent with the widely accepted estimated size of Veneneia basin (e.g., Jaumann et al., 2012; Marchi et al., 2012; Schenk et al., 2012).

Visual inspection of our mapped structures reveals a partly preserved clockwise spiral pattern of basin structures extending from the central mound to the rim (Figure 6). The pattern is most distinctly expressed by scarps and ridges, but some lineaments also follow the same structural trend on the Rheasilvia basin floor outside of the estimated area of the Veneneia basin floor. Scarps mostly face the basin center along and near the basin-bounding scarps. There, they show a pattern concentric to the basin center, but they systematically deviate from this concentric pattern closer to the center of the basin. This pattern is the most distinct and systematic in the eastern part of the basin between 60°E to 150°E. The occurrence of ridges is sparse near the basin-bounding scarps at 0° to 60°E and 120°E to 180°, but they are densely distributed at the low-lying basin floor between the central mound and basin slope. Some ridges follow the spiral pattern of the scarps, such as the curved ridges observed at 60°E to 120°E. The pattern of scarps and ridges is less systematic at the western part of the basin at 30°W to 120°W, which we attribute to structures that pre-existed from the now superposed Veneneia basin (Figure 6). Although some undefined lineaments follow the orientations of scarp and basins locally, they generally do not follow the spiral pattern.

3.2. Orientation of each type of structure

To assess the orientation of each type of structure, the basin was subdivided into bins using three concentric circles with radii of 100 km, 200 km, and 300 km from the calculated basin center. Those concentric bins were subdivided into 12 radial bins, resulting in 36 regional bins around the basin center. Length-weighted rose diagrams were plotted for the three types of structures in each bin to visualize their orientations across the basin to aid our assessment of the structural patterns (Figure 7).

The basin-bounding scarps are large concentric structures around the basin center as seen on both the structural map and rose diagrams (Figure 7a,b). Deviations from the concentric pattern are most pronounced in the Rheasilvia basin that superposes the Veneneia basin. The intra-basin scarps form a pervasive spiral pattern within the basin, especially near the basin-bounding scarps (Figure 7a). The rose diagrams quantitatively capture the spiral pattern with the scarps furthest from the basin center showing distinctively concentric orientations, but their orientation increasingly and systematically deviates from this concentric orientation closer to the basin center (Figure 7b).

Ridges are less prominent than scarps, as they have shorter individual lengths and their pattern relative to the basin center is not as well defined as the scarps (Figure 7c). Overall, the ridges show concentric and, in a few places, radial orientations to the basin center with concentric orientations mostly near the basin-bounding scarps (Figure 7d). There are regional bins that show ridge orientations like those of the scarps (Figure 7b), but they do not form an obvious spiral pattern throughout the basin. The ridges between latitudes of 30^{o}S to 60^{o}S and longitudes of 0^{o} to 90^{o}E show a regional fabric trending roughly from east and west (Figure 7c). This pattern is also captured by the rose diagrams with a high density of ridge segments (Figure 7d).

Undefined lineaments are widely and densely distributed across the basin floor (Figure 7e). Most are relatively short compared to ridges and scarps, and they form no distinctive map patterns. Rose diagrams show that the undefined lineaments display preferred orientations in all regional bins (Figure 7f). There are regional bins that show radial and concentric patterns with respect to the basin center, but they do not form a consistent pattern across all bins, such that no systematic pattern is present throughout the basin. Some undefined lineaments between the latitudes of 30^{o}S to 60^{o}S and longitudes of 0^{o} to 90^{o}E mimic the regional fabric of ridges (Figure 7c) trending roughly from east and west (Figure 7e).

Lighting may potentially impose a bias on the detectability of structures. Where solar illumination is parallel to the structure, the contrast in illumination of the structure is so low as to render the structure nearly invisible, whereas a structure approximately perpendicular to this direction is prominently visible on the FC images. The mapping of scarps and ridges was verified with hillshades created from multiple azimuths (Figures 2, 3, and 4), but the undefined lineaments could not be verified (Figure 5). Thus, the preferred orientations of ridges and scarps have no or minimal lighting influence and can be accounted for the tectonics of the basin. However, preferred orientations of undefined lineaments may be biased by the lighting of FC images, and they may not fully characterize the tectonics of the basin.

<insert Figure 7>

3.3. Density of structures

We analyzed the density of each type of structure within the Rheasilvia basin. Each structure was split at its vertices into ~1 km long segments. The splitting ensures that longer structures are more prominently represented in our density calculation because longer structures will return more segments. The coordinate of the centroid of each segment was calculated, and the number of centroids per square kilometer was computed for each type of structure using the *Kernel Density Calculates function*, which calculates the density of point features around each output raster cell in an equal area stereographic projection. Basin-bounding scarps were not considered for this calculation, as they would weigh scarps more heavily along the basin boundary.

Basin structures are densely distributed across almost the entire basin floor. Some areas near post-Rheasilvia impact craters or at the downslope of scarps (e.g., Matronalia Rupes and the central mound-bounding scarps) show only undefined lineaments or no structures (Figures 6 and 8). These smoother areas are possibly covered with resurfaced materials produce by impacts or by landslides. The density of the scarps is highest between 80°E to 150°E along the latitude of 30°S. The scarps have a high density (dark red in Figure 8a) on the basin floor that slopes toward the basin center, where they are associated with the basin-bounding scarps, and they show a low density on the flat basin floor near the central mound (light red in Figure 8a).

Ridges show a low density near the central mound and near the basin-bounding scarps (light blue in Figure 8b) but they cluster between these two regions on the flat basin floor (dark blue in Figure 8b), encircling the central mound. Hence, scarps and ridges show an opposite spatial distribution, with scarps densely located near the basin perimeter surrounding a group of ridges at the basin floor around the central mound (Figure 8a and b). Undefined lineaments show a less distinct pattern in their spatial density with some of them densely located near the basin-bounding scarps (Figure 8c). Regions of low structural density occur where superposed impact craters are recorded, and thus resurfacing has occurred and erased the expressions of this structure type.

<insert Figure 8>

3.4. Cross-cutting relationships

The three types of structures in the Rheasilvia basin lack a systematic pattern of cross-cutting relationships. An example of an area displaying wide variation in cross-cutting relationships is shown in Figure 9. These relationships (all labeled in Figure 9c) include one basin-bounding scarp truncating a large scarp within the basin (1), that large scarp cutting smaller scarps (2) and ridges (3), and a ridge abutting that large scarp (4). Such mutually cross-cutting relationships are present across the entire basin floor (Figure 6), indicating that all these structure types formed simultaneously and not sequentially.

<insert Figure 9>

Scarps and ridges are in all cases superposed by impact craters (Figure 6), indicating that the structures were formed before the craters were emplaced. Most undefined lineaments are also superposed by impact craters, but in places, they cross-cut crater floors (Figure 6). This shows that most lineaments were formed before the emplacement of the craters, but also that their formation continued locally for some time.

The southernmost trough belonging to the Divalia Fossae cuts the Rheasilvia basin-bounding scarps and lies partly within the basin. The relationship is most obvious in the hillshade images (Figure 2b,d) that differ the most in illumination conditions as compared to the natural lighting in the FC images. The trough is not cut by any of the scarps and ridges, but it is cut by undefined lineaments (Figures 6). That the trough cuts the basin-bounding scarp and basin floor but is not cut itself by scarps and ridges indicates that the trough formed after the emplacement of the Rheasilvia basin and after the formation of all major basin interior structures. This heretofore unrecognized cross-cutting relationship adds crucial information to the interpretation of the origin of the troughs. We will explore the basin and trough relationship further in the next section.

4. Spatial Relationship of Rheasilvia basin and Divalia Fossae

With no cross-cutting relationships previously described, the Rheasilvia basin and Divalia Fossae were widely considered to be genetically linked because of the spatial correlation of the basin center with the poles to vertical planes projected through the troughs. We have plotted the Divalia Fossae and their associated pit-crater chains from Cheng and Klimczak (2022) with the Rheasilvia basin-bounding scarps and basin center of this study (Figure 6). This map highlights the spatial relationship of the basin and throughs that include the southernmost trough of the Divalia Fossae cutting into the Rheasilvia basin. This newly recognized cross-cutting relationship suggests that this trough, and likely the entire Divalia Fossae structure, was formed after the emplacement and modification of the Rheasilvia basin.

<insert Figure 10>

The Divalia Fossae do not show an obvious concentric arrangement around the Rheasilvia basin (Figure 10). To evaluate their arrangement, we determined the planes defined by the Divalia Fossae using two methods and plotted their poles with the basin centers on an equal-area stereonet (Figure 11). *Method 1* follows the procedure described in Jaumann et al. (2012), in which the planes defined by the troughs are assumed to be vertical, cutting through the center of the asteroid. The orientations of the planes located at the center positions of each of the trough segments are shown as great circles in an equal area stereonet (Figure 11a). The poles of the trough-defined planes are clustered around the center of the stereonet, mostly consistent with the result from Jaumann et al. (2012). The two basin centers determined by Jaumann et al. (2012) and this study lie outside of the 95% confidence interval of these poles, but the south pole of Vesta lies within it.

Since the planes defined by the Divalia Fossae troughs may not cut through the center of the asteroid, we also use *Method 2*, which determines the planes defined by the troughs without the assumption that they cut through the center of the asteroid. The trough segments of Divalia Fossae belong to four main trough structures (Figures 8; Cheng and Klimczak, 2022), and we use those four structures to redefine the planes. To determine the circular shape that best fits each structure, we used the three-point method in the *CraterTools plug-in* (Kneissl et al., 2011) that has a built-in projection correction by identifying the starting, middle, and ending points along the four structures. These circular planes are represented as small circles on an equal-area stereonet (Figure 11b), showing that these planes do not cut through the center of the asteroid.

We calculated the center locations of these circular planes to plot their poles. The poles of the trough-defined planes cluster near the center of the stereonet, which coincides with Vesta's south pole. Like the results for *Method 1* (Figure 11a), the two basin centers lie outside of the 95% confidence interval of the poles, but the south pole of Vesta lies within it.

Similarly, troughs and basin-bounding scarps also indicate that Divalia Fossae are not concentrically arranged around the Rheasilvia basin (Figure 10). Furthermore, our structural analysis indicates that the basin center does not fall within the 95% confidence limit of the poles of the troughs, irrespective of the method of how the poles are determined and what coordinates define the basin center in the different studies. Therefore, it is with 95% probability that the basin center is not co-located with the pole of the troughs. These lines of evidence indicate that the Rheasilvia basin and the Divalia Fossae do *not* show a direct and clearly defined spatial relationship.

<insert Figure 11>

5. Discussion

5.1. Basin structures and their formation processes

The structural map of the Rheasilvia basin presented in this study (Figure 6) allows us to conduct spatial analyses and assessments of the orientation of several types of structures found in and around this large impact structure. These results of our analyses have implications for the geologic processes that took place within the basin. Basin-bounding scarps, such as Matronalia Rupes, are interpreted as the main scarp resulting from major mass-wasting events (Otto et al., 2013). Numerous scarps within the basin represent ruptures along which slumping took place, with ridges in the front of the slump representing the toes of the slumping masses (Otto et al., 2013). This interpretation is consistent with our observation that the scarps facing the basin center are clustered near the basin-bounding scarps at the perimeter of the Rheasilvia basin (Figure 8a), and the spatial density of ridges is higher closer toward the basin center on the basin floor around the central mound (Figure 8b), displaying an anti-correlation in their spatial distribution. This indicates the mass movement of basin material from the basin rim towards the floor, which is likely caused by the gravitational collapse and modification resulting from the impact forming the basin. This interpretation is supported by the detailed observations of the nature and orientations of mass-wasting landforms within the basin (Otto et al., 2013).

The scarps and ridges are mutually cross-cutting across the basin (Figures 6 and 9), indicating there are episodic mass-wasting events across the basin, without a sequence of events or specific temporal order of the mapped structure types. Since the scarps and ridges are all superposed by impact craters inside the basin (Figure 6), they must have formed prior to the superposition of the impact craters, likely soon after the emplacement of the Rheasilvia basin, with most mass wasting being complete shortly after basin formation. Otto et al. (2013) reported young slides and slumps at the Matronalia Rupes scarp, and he suggested they demonstrate the ongoing collapse of the basin. In contrast, we find that this interpretation does not reflect most mass-wasting that occurred in the basin.

Scarps display a well-preserved clockwise spiral pattern extending from the central mound to basin rim between 60°E and 150°E, coinciding with the area that does not superpose the Veneneia basin floor (Figure 7a and b). Some ridges in this area also follow the same structural trend locally (Figure 6). One possible explanation for this structural pattern is that the curved structures are remnants of the basin-collapse process when materials moving from the rim to the floor radially were deflected by the Coriolis effect (Jutzi et al., 2013; Otto et al., 2013;

2016). Otto et al. (2016) interpreted the spiral patterns as ‘curved ridges’ of materials deposited along the predominant slope from the basin rim to the floor during the basin modification stage. The velocities of mass movement derived along these ‘curved ridges’ were calculated by assuming they were caused by the Coriolis effect (Otto et al., 2016), which generally agrees with the predicted mass motion velocity from numerical simulations (Jutzi et al., 2013). These “curved ridges” on a large-scale map consist of scarps and ridges based on our structural map (Figure 6). If the scarps represent rupture during slumping and the Coriolis effect is responsible for the spiral pattern, the Coriolis force may not just deflect the movement of slumping materials but also influence the preceding rupture during basin collapse.

However, the spiral pattern of the Rheasilvia basin should be expected to extend from the south pole of Vesta under the Coriolis effect, instead of the center of the impact basin. From the preserved structures we mapped, it is impossible to distinguish if the spiral pattern is centered around the south pole or the Rheasilvia basin (Figure 6). Schenk et al. (2022) reported that spiral patterns are common to complex craters on Moon, Mars, Mercury, Ceres, and other icy bodies, which are not located near the poles. As such, the Coriolis effect does not need to be invoked to form the spiral pattern on the Rheasilvia basin. The crater examples given by Schenk et al. (2022) range in diameter from 9 to 66 km, which are much smaller than the 450-km-diameter Rheasilvia basin, and they thus have much lower size ratios relative to their parent bodies. Furthermore, the reported spiral patterns in these smaller craters were selected from visual inspection without structural analysis and they are mostly partially preserved, as the crater floors are buried by impact melt and debris. Therefore, these craters are likely not analogous to the Rheasilvia basin and its pervasive spiral deformation pattern, leaving the Rheasilvia spiral pattern as uncommon among large impact structures in the solar system.

The spiral pattern is not present on the western side of the Rheasilvia basin, where it is estimated to superpose the Veneneia basin (Figure 6). Any pre-existing Veneneia basin structures likely substantially influenced the orientations of structures in the Rheasilvia basin. In this case, the Veneneia basin floor and its structures would have been planes of weakness during the Rheasilvia impact. Thus, Vesta's lithosphere must have been highly fractured by the Veneneia impact, and it remained highly fractured until the Rheasilvia basin was emplaced. Any fracture healing and fracture annealing caused by shock residual or interior heat is therefore unlikely to have occurred on the Veneneia basin floor. This absence is possible if the Veneneia basin formed from a low-velocity impactor, similar to that proposed for the Rheasilvia impact (O'Brian and Sykers, 2011). This scenario is consistent with the lack of a melt sheet associated with the Veneneia impact on the preserved part of the basin.

5.2. Origin of the Divalia Fossae

The Divalia Fossae are widely accepted to have formed directly by the impact that formed the Rheasilvia basin (e.g, Buczkowski et al., 2012; Jaumann et al., 2012; Scully et al., 2014; Schäfer et al., 2014; Williams et al., 2014; Yingst et al., 2014). This scenario solely relied on the geographic relationship that the Divalia Fossae showed with respect to the center of the Rheasilvia basin (Jaumann et al., 2012; Scully et al., 2014; Schäfer et al., 2014). Our reassessment of this geographic relationship indicates that the geometric mean center of the basin does not lie within the 95% confidence ellipse defined by the locations of the poles of the planes along the Divalia Fossae (Figure 11). Therefore, it is with 95% probability that the basin center is not co-located with the pole of the troughs. This result establishes that the Divalia Fossae do not display a direct and clearly defined geographic relationship with the Rheasilvia basin, and thus it cannot be used as evidence supporting the basin-forming impact triggering the formation of the troughs that constitute the Divalia Fossae.

The previously proposed origin of the troughs is further challenged by the newly identified cross-cutting relationship that the Divalia Fossae and Rheasilvia basin-bounding scarps display. The southernmost trough of the Divalia Fossae cuts the basin-bounding scarp and lies partly within the basin without being crosscut by the scarps and ridges in the basin interior (Figures 4 and 8), indicating that the troughs must be formed after the emplacement and modification of Rheasilvia. The emplacement and modification of the Rheasilvia basin were estimated to take place over approximately 2 to 3 hours (Jutzi et al., 2013; Ivanov and Melosh, 2013; Otto et al., 2016). In contrast, typical earthquake rupture propagation rates of approximately 3 km/s (Stein and Wysession, 2003) imply that fractures that formed deep within Vesta from the Rheasilvia impact propagated to the surface after ~100–150 s (Stickle et al., 2015). Following the results of these studies, the formation of Divalia Fossae, if caused by the Rheasilvia impact, would take place before the modification stage of the Rheasilvia basin was completed, which contradicts the cross-cutting relationship. Our geologic observations require for the Divalia Fossae to be formed after the basin modification stage, questioning the previously proposed impact-induced origin of the Divalia Fossae.

It is widely accepted that large impacts can form major structures at the antipodes (e.g., Schultz and Gault, 1975; Murray et al., 1974; Melosh and McKinnon, 1988); however, no such structures on Vesta and Divalia Fossae occur at the antipode. Blewett et al. (2014) found that the cratered highland near the north pole of Vesta is likely to be a remnant of ancient crust formed before the Rheasilvia impact, and no large-scale troughs were observed there. While several reasons may explain the lack of major antipode structures, such as weakened antipodal constructive interference of seismic waves due to an oblique impact, the non-spherical shape of Vesta, or the physical properties of the interior (Blewett et al., 2014), it remains an open question of how structures as large scale as Divalia Fossae could have formed away from the antipode, yet be directly caused by the impact.

The Divalia Fossae are concentric around the south pole of Vesta and the south pole falls within the 95% confidence ellipse of the poles to planes through the troughs (Figures 10 and 11), establishing a geographic relationship with Vesta's spin axis. The asteroid is spinning rapidly with a well-determined rotational period of 5.342 hours, and it has a marked equatorial bulge and polar flattening. An origin of the Divalia Fossae related to Vesta's spinning has previously been proposed, including spinning-up of the asteroid and reorientation of the spin axis by the Rheasilvia impact (Schmidt, 2011). These hypotheses suggest the Divalia Fossae were formed by long-term consequences of asteroid tectonics after the Rheasilvia impact, which are permissible with the cross-cutting relationships shown here and previously derived age relationships from crater statistics (Cheng et al., 2021).

In particular, the crater statistics were derived for the Divalia Fossae and compared with those of the Rheasilvia basin to determine their relative age (Cheng et al., 2021). Although the reported crater frequencies permit a simultaneous formation of the two landforms, large uncertainties allow for the Divalia Fossae to have formed well before or after the emplacement of the Rheasilvia basin (Cheng et al., 2021). Since the southernmost trough of the Divalia Fossae cuts the basin-bounding scarp and lies partly within the basin (Figures 6 and 10), the age of formation of the Divalia Fossae can be constrained to after the Rheasilvia basin was formed.

Crater-counting studies interpreted that the Rheasilvia basin formed at ~0.8 Ga to 3.5 Ga. Crater counting of the entire basin floor (Marchi et al., 2012; Schenk et al., 2012) estimated the basin age to be ~1 Ga and ~1.8 Ga, based on the Main Belt crater production function (O'Brien et al., 2007) and lunar-derived crater production function (Schmedemann et al., 2014), respectively. A different crater counting study (Schmedemann et al., 2014) produced a basin age of ~3.5 Ga. A recently updated crater count and interpretation of Rheasilvia suggests a much younger basin age of ~0.8 to 0.9 Ga (Schenk et al., 2022). If the Rheasilvia basin is indeed very young, the trough that crosscuts it must be even younger. However, the Divalia Fossae are heavily degraded (Cheng and Klimczak, 2022), which argues against the young age interpretation of the Rheasilvia basin.

Hypotheses that would tie the tectonics of Vesta to long-term consequences of the Rheasilvia impact include the possibility of asteroid reorientation (e.g., Karimi and Dombard, 2016). In particular, the study numerically modeled the potential for relaxation of large south polar basins and a rotational bulge after the asteroid reoriented. The models predict that Vesta’s lithosphere was too cold to permit the relaxation basin topography and the rotational bulge at a time after basin formation, and thus reorientation of Vesta by the Rheasilvia impact is unlikely to have happened (Karimi and Dombard , 2016). Alternatively, Mao and McKinnon (2020) suggested that Vesta likely spun up based on the scale and location of the Rheasilvia impact, which was suggested in this study to have played a role in forming the Divalia and Saturnalia Fossae. The specifics of this scenario for the formation of the Divalia Fossae have yet to be investigated. Our findings challenge the previously proposed origin of the Divalia Fossae, that they were caused directly by the Rheasilvia impact. Future studies may need to consider alternative hypotheses that satisfy the geographic, cross-cutting, and age relationships we presented here.

6. Conclusions

We produced a detailed structural map of the Rheasilvia basin to characterize the various structures using rigorous mapping criteria with the aim of quantitively analyzing the orientations, densities, and cross-cutting relationships of these structures. The basin surface is dominated by scarps near the basin rim and ridges on the basin floor near the central mound. Scarps display a well-preserved clockwise spiral pattern extending from the central mound to basin rim in the eastern part of the basin, with some ridges locally following the same structural trend. This pattern was previously interpreted as modification of the basin by mass-wasting, influenced by the Coriolis effect during the basin modification and collapse. The scarps and ridges lack a clear systematic pattern in the area coinciding with the superposed Veneneia basin, indicating that pre-existing Veneneia structures substantially influenced the orientation of Rheasilvia-associated structures. This indicates that the lithosphere must have been shattered by the Veneneia impact, and that no healing and annealing occurred before the impact that formed the Rheasilvia basin.

The Rheasilvia basin structural map shows that the Divalia Fossae crosscut the basin-bounding scarps, which has not been previously recognized. Likewise, the configuration of the Rheasilvia basin and Divalia Fossae, in contrast to conclusions of previous studies, are not geographically correlated. The cross-cutting relationship and configuration of the Rheasilvia basin and Divalia Fossae greatly challenge the widely accepted hypothesis that the Divalia Fossae were formed directly by the Rheasilvia impact. Taken together with established age relationships, the Divalia Fossae are more likely to have formed as a long-term consequence of the Rheasilvia impact tied to changes in rotation of the asteroid, supporting previously discarded hypotheses of an impact-induced up-spinning or reorientation of Vesta around its spin axis. The relationships between the Divalia Fossae and Rheasilvia basin established here serve as geologic constraints that must be accounted for when assessing hypotheses that seek to understand the tectonic evolution of Vesta.

Acknowledgments

The supplemental shapefiles of this manuscript are available at https://data.mendeley.com/datasets/bxbykxrk7h/1.

References

Allmendinger, R.W., Cardozo, N.C., and Fisher, D., 2013. *Structural Geology Algorithms: Vectors & Tensors*. Cambridge, England, Cambridge University Press.

Asphaug, E., 1997. Impact origin of the Vesta family. *Meteoritics & Planetary Science*, *32*(6), pp.965-980.

Asphaug, E., Moore, J. M., Morrison, D., Benz, W., Nolan, M. C. and Sullivan, R. J., 1996. Mechanical and geological effects of impact cratering on Ida. *Icarus*, *120*(1), pp.158-184.

Benz, W. and Asphaug, E., 1994. Impact simulations with fracture. I. Method and tests. *Icarus*, *107*(1), pp.98-116.

Blewett, D.T., Buczkowski, D.L., Ruesch, O., Scully, J.E., O'Brien, D.P., Gaskell, R., Roatsch, T., Bowling, T.J., Ermakov, A., Hiesinger, H. and Williams, D.A., 2014. Vesta's north pole quadrangle Av-1 (Albana): Geologic map and the nature of the south polar basin antipodes. *Icarus*, *244*, pp.13-22.

Bowling, T.J., Johnson, B.C. and Melosh, H.J., 2014. Formation of equatorial graben on 4 Vesta following the Rheasilvia basin forming impact. *Vesta in the Light of Dawn: First Exploration of a Protoplanet in the Asteroid Belt*, *1773*, 2018.

Buczkowski, D.L., Wyrick, D.Y., Iyer, K.A., Kahn, E.G., Scully, J.E.C., Nathues, A., Gaskell, R.W., Roatsch, T., Preusker, F., Schenk, P.M. and Le Corre, L., 2012. Large-scale troughs on Vesta: A signature of planetary tectonics. *Geophysical Research Letters*, *39*(18).

Cardozo, N. and Allmendinger, R.W., 2013. Spherical projections with OSXStereonet. *Computers & Geosciences*, *51*, pp.193-205.

Cheng, H.C.J. and Klimczak, C., 2022. The large-scale troughs on Asteroid 4 Vesta accommodate opening-mode displacement. *EarthArXiv*. https://doi.org/10.31223/X51G6T.

Cheng, H.C.J., Klimczak, C. and Fassett, C.I., 2021. Age relationships of large-scale troughs and impact basins on Vesta. *Icarus*, *366*, pp.114512.

Collins, G.S., Morgan, J., Barton, P., Christeson, G.L., Gulick, S., Urrutia, J., Warner, M. and Wünnemann, K., 2008. Dynamic modeling suggests terrace zone asymmetry in the Chicxulub crater is caused by target heterogeneity. *Earth and Planetary Science Letters*, *270*(3-4), pp.221-230.

Drake, M.J. and Consolmagno, G.J., 1977. Asteroid 4 Vesta: Possible bulk composition deduced from geochemistry of eucrites. In *Lunar and Planetary Science Conference* (Vol. 8).

Ivanov, B.A. and Melosh, H.J., 2013. Two-dimensional numerical modeling of the Rheasilvia impact formation. *Journal of Geophysical Research: Planets*, *118*(7), pp.1545-1557.

Jaumann, R., Williams, D.A., Buczkowski, D.L., Yingst, R.A., Preusker, F., Hiesinger, H., Schmedemann, N., Kneissl, T., Vincent, J.B., Blewett, D.T. and Buratti, B.J., 2012. Vesta's shape and morphology. *Science*, *336*(6082), pp.687-690.

Jutzi, M., Asphaug, E., Gillet, P., Barrat, J.A. and Benz, W., 2013. The structure of the asteroid 4 Vesta as revealed by models of planet-scale collisions. *Nature*, *494*(7436), pp.207-210.

Karimi, S. and Dombard, A.J., 2016. On the possibility of viscoelastic deformation of the large south polar craters and true polar wander on the asteroid Vesta. *Journal of Geophysical Research: Planets*, *121*(9), pp.1786-1797.

Kneissl, T., van Gasselt, S. and Neukum, G., 2011. Map-projection-independent crater size-frequency determination in GIS environments—New software tool for ArcGIS. *Planetary and Space Science*, *59*(11-12), pp.1243-1254.

Krohn, K., Jaumann, R., Otto, K., Hoogenboom, T., Wagner, R., Buczkowski, D.L., Garry, B., Williams, D.A., Yingst, R.A., Scully, J. and De Sanctis, M.C., 2014. Mass movement on Vesta at steep scarps and crater rims. *Icarus*, *244*, pp.120-132.

Li, J.Y. and Mafi, J.N. (2012). Body-fixed coordinate systems for Asteroid (4) Vesta. *Planetary Data System*.

Liu, Z., Yue, Z., Michael, G., Gou, S., Di, K., Sun, S. and Liu, J., 2018. A global database and statistical analyses of (4) Vesta craters. *Icarus*, *311*, pp.242-257.

Mao, X. and McKinnon, W.B., 2020. Spin evolution of Ceres and Vesta due to impacts. *Meteoritics & Planetary Science*, *55*(11), pp.2493-2518.

Marchi, S., McSween, H.Y., O’Brien, D.P., Schenk, P., De Sanctis, M.C., Gaskell, R., Jaumann, R., Mottola, S., Preusker, F., Raymond, C.A. and Roatsch, T., 2012. The violent collisional history of asteroid 4 Vesta. *Science*, *336*(6082), pp.690-694.

Marzari, F., Cellino, A., Davis, D.R., Farinella, P., Zappala, V. and Vanzani, V., 1996. Origin and evolution of the Vesta asteroid family. *Astronomy and Astrophysics*, *316*, pp.248-262.

McCord, T.B., Adams, J.B. and Johnson, T.V., 1970. Asteroid Vesta: Spectral reflectivity and compositional implications. *Science*, *168*(3938), pp.1445-1447.

Melosh, H.J., 1989. *Impact cratering: A geologic process*. New York: Oxford University Press; Oxford: Clarendon Press.

Melosh, H.J. and McKinnon, W.B., 1988. The tectonics of Mercury. *Mercury, University of Arizona Press,* pp.374-400.

Meschede, M.A., Myhrvold, C.L. and Tromp, J., 2011. Antipodal focusing of seismic waves due to large meteorite impacts on Earth. *Geophysical Journal International*, *187*(1), pp.529-537.

Murray, B.C., Belton, M.J., Danielson, G.E., Davies, M.E., Gault, D.E., Hapke, B., O'Leary, B., Strom, R.G., Suomi, V. and Trask, N., 1974. Mercury's surface: Preliminary description and interpretation from Mariner 10 pictures. *Science*, *185*(4146), pp.169-179.

O’Brien, D.P. and Sykes, M.V., 2011. The origin and evolution of the asteroid belt—Implications for Vesta and Ceres. *Space science reviews*, *163*(1-4), pp.41-61.

Otto, K.A., Jaumann, R., Krohn, K., Matz, K.D., Preusker, F., Roatsch, T., Schenk, P., Scholten, F., Stephan, K., Raymond, C.A. and Russell, C.T., 2013. Mass-wasting features and processes in Vesta's south polar basin Rheasilvia. *Journal of Geophysical Research: Planets*, *118*(11), pp.2279-2294.

Otto, K.A., Jaumann, R., Krohn, K., Spahn, F., Raymond, C.A. and Russell, C.T., 2016. The Coriolis effect on mass wasting during the Rheasilvia impact on asteroid Vesta. *Geophysical Research Letters*, *43*(24), pp.12-340.

Pieters, C.M., Ammannito, E., Blewett, D.T., Denevi, B.W., De Sanctis, M.C., Gaffey, M.J., Le Corre, L., Li, J.Y., Marchi, S., McCord, T.B. and McFadden, L.A., 2012. Distinctive space weathering on Vesta from regolith mixing processes. *Nature*, *491*(7422), pp.79-82.

Poelchau, M.H. and Kenkmann, T., 2008. Asymmetric signatures in simple craters as an indicator for an oblique impact direction. *Meteoritics & Planetary Science*, *43*(12), pp.2059-2072.

Preusker, F., Scholten, F., Matz, K.D., Roatsch, T., Jaumann, R., Raymond, C.A. and Russell, C.T., 2016. DAWN FC2 DERIVED VESTA DTM SPG V1.0, DAWN-A-FC2-5-VESTADTMSPG-V1.0, *NASA Planetary Data System.*

Roatsch, T., Kersten, E., Matz, K.D., Preusker, F., Scholten, F., Elgner, S., Schroeder, S.E., Jaumann, R., Raymond, C.A. and Russell, C.T., 2015. Dawn FC2 derived vesta global mosaics V1. 0. *NASA Planetary Data System*, DAWN-A.

Russell, C.T. and Raymond, C.A., 2011. The dawn mission to Vesta and Ceres. *The dawn mission to minor planets 4 vesta and 1 ceres*, pp.3-23.

Russell, C.T., Raymond, C.A., Coradini, A., McSween, H.Y., Zuber, M.T., Nathues, A., De Sanctis, M.C., Jaumann, R., Konopliv, A.S., Preusker, F. and Asmar, S.W., 2012. Dawn at Vesta: Testing the protoplanetary paradigm. *Science*, *336*(6082), pp.684-686.

Schäfer, M., Nathues, A., Williams, D.A., Mittlefehldt, D.W., Le Corre, L., Buczkowski, D.L., Kneissl, T., Thangjam, G.S., Hoffmann, M., Schmedemann, N. and Schäfer, T., 2014. Imprint of the Rheasilvia impact on Vesta–Geologic mapping of quadrangles Gegania and Lucaria. *Icarus*, *244*, pp.60-73.

Schenk, P.M., Neesemann, A., Marchi, S., Otto, K., Hoogenboom, T., O'Brien, D.P., Castillo-Rogez, J., Raymond, C.A. and Russell, C.T., 2021. A young age of formation of Rheasilvia basin on Vesta from floor deformation patterns and crater counts. *Meteoritics & Planetary Science*, *57*(1), pp.22-47

Schenk, P., Vincent, J.B., O'Brien, D.P., Jaumann, R. and Williams, D., 2012, September. Impact crater morphologies on Vesta. In *European Planetary Science Congress* (Vol. 7, pp. 700).

Schmidt, B.E., 2011, December. Tectonics of Vesta: Indication of Spin-up and Reorientation?. In *AGU Fall Meeting Abstracts* (Vol. 2011, pp. U21B-06).

Schultz, P.H. and Crawford, D.A., 2011. Origin of nearside structural and geochemical anomalies on the Moon. *Geological Society of America Special Papers*, *477*, pp.141-159.

Schultz, P.H. and Gault, D.E., 1975. Seismic effects from major basin formations on the Moon and Mercury. *The Moon*, *12*(2), pp.159-177.

Scully, J.E., Yin, A., Russell, C.T., Buczkowski, D.L., Williams, D.A., Blewett, D.T., Ruesch, O., Hiesinger, H., Le Corre, L., Mercer, C. and Yingst, R.A., 2014. Geomorphology and structural geology of Saturnalia Fossae and adjacent structures in the northern hemisphere of Vesta. *Icarus*, *244*, pp.23-40.

Sierks, H., Keller, H.U., Jaumann, R., Michalik, H., Behnke, T., Bubenhagen, F., BŘttner, I., Carsenty, U., Christensen, U., Enge, R. and Fiethe, B., 2011. The Dawn framing camera. *Space science reviews*, *163*(1-4), pp.263-327.

Stein, S. and Wysession, M., 2009. *An introduction to seismology, earthquakes, and earth structure*. John Wiley & Sons.

Stickle, A.M., Schultz, P.H. and Crawford, D.A., 2015. Subsurface failure in spherical bodies: A formation scenario for linear troughs on Vesta's surface. *Icarus*, *247*, pp.18-34.

Thomas, P.C., Binzel, R.P., Gaffey, M.J., Zellner, B.H., Storrs, A.D. and Wells, E., 1997. Vesta: Spin pole, size, and shape from HST images. *Icarus*, *128*(1), pp.88-94.

The IAU WG Cartographic Coordinates & Rotational Elements (WGCCRE) (2014). New Coordinate System for (4) Vesta.

Williams, D.A. and Greeley, R., 1994. Assessment of antipodal-impact terrains on Mars. *Icarus, 110*(2), pp.196-202.

Williams, D.A., Jaumann, R., McSween Jr, H.Y., Marchi, S., Schmedemann, N., Raymond, C.A. and Russell, C.T., 2014. The chronostratigraphy of protoplanet Vesta. *Icarus, 244*, pp.158-165.

Wilson, L. and Head, J.W., 2015. Groove formation on Phobos: Testing the Stickney ejecta emplacement model for a subset of the groove population. *Planetary and Space Science*, *105*, pp.26-42.

Yingst, R.A., Mest, S.C., Berman, D.C., Garry, W.B., Williams, D.A., Buczkowski, D., Jaumann, R., Pieters, C.M., De Sanctis, M.C., Frigeri, A.L. and Le Corre, L., 2014. Geologic mapping of Vesta. *Planetary and Space Science*, *103*, pp.2-23.

Figures and captions

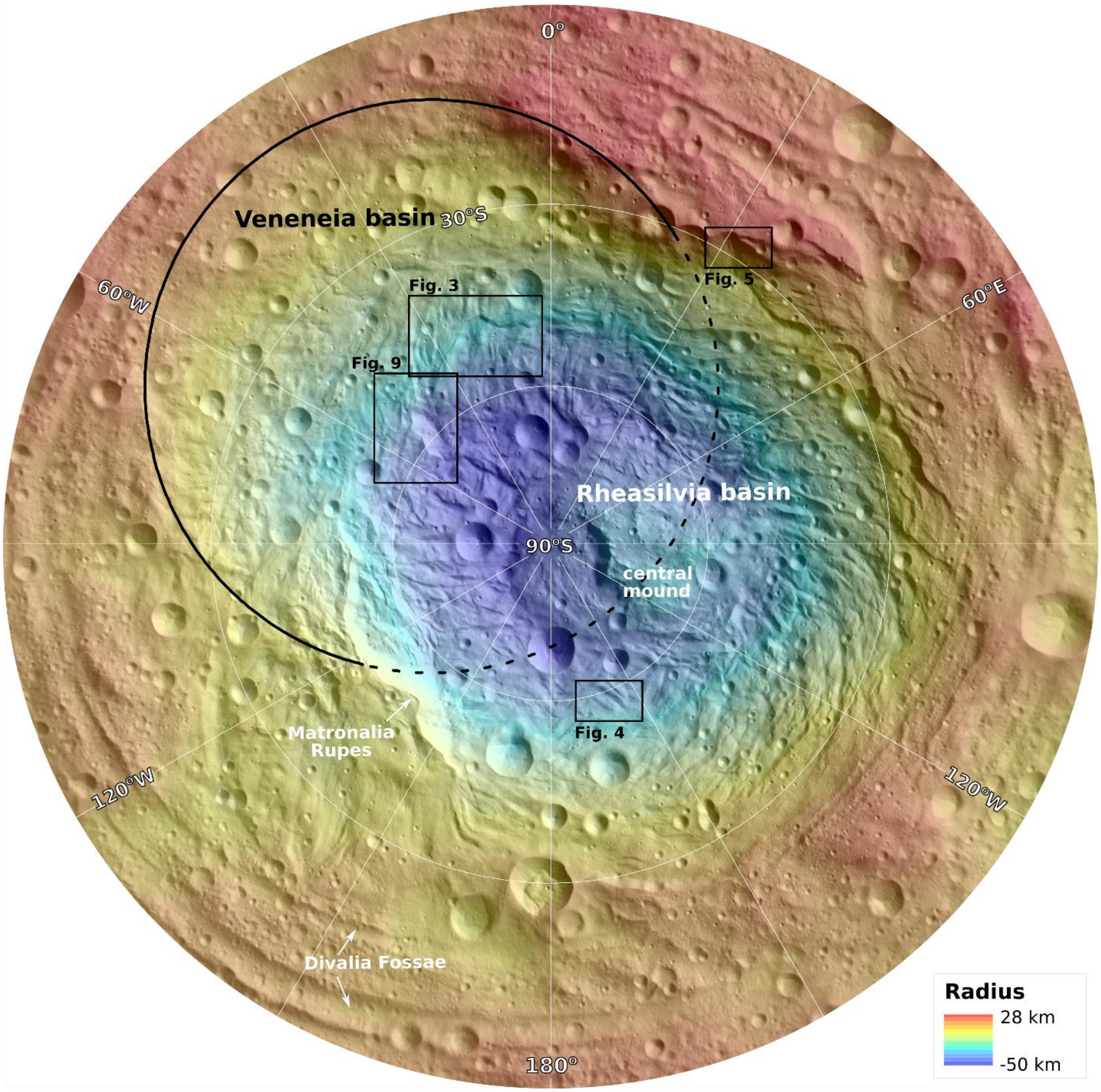

Figure 1. Location map of the Rheasilvia and Veneneia basins displayed as hillshade generated from the Dawn Digital Elevation Model (DEM) with the solar azimuth of 56°E and incidence angle of 45° (same as Figure 2a) color-coded by elevation in south polar stereographic projection. The reference elevation is defined to be the mean planetary radius of 262 km. The estimated circular basin rim of Veneneia basin is outlined with the preserved part in black solid

line and the part superposed by the Rheasilvia basin in black dotted line. The location of the Divalia Fossae, the Rheasilvia central mound, and Matronalia Rupes are also indicated. <2-columns, color>

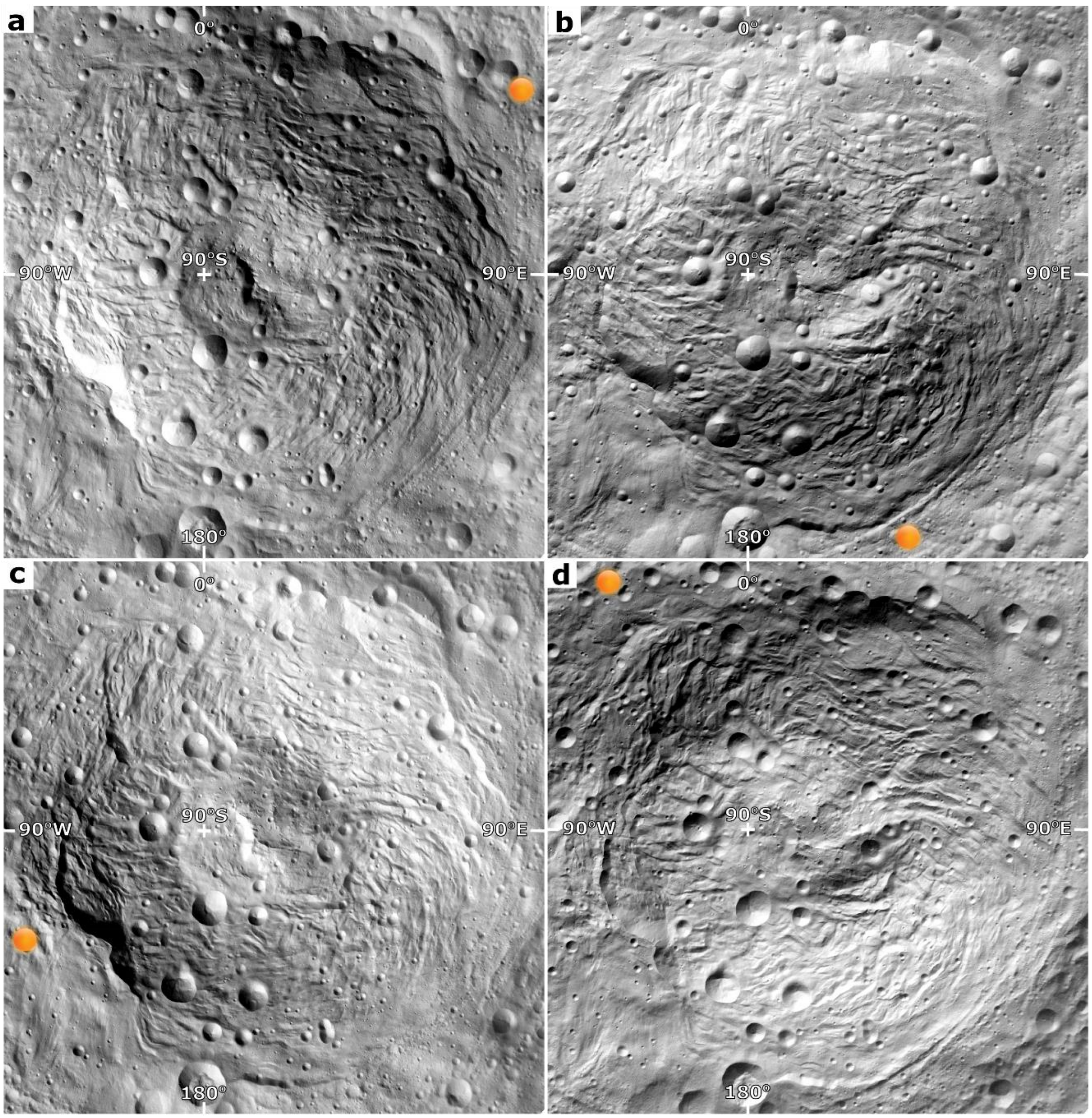

Figure 2. Hillshade maps of Rheasilvia Basin generated from the Dawn Digital Elevation Model (DEM) with four azimuths (the angular directions of the sun) and a fixed solar incidence angle of

45°. The four azimuths we used include (a) 56°E, (b) 146°E, (c) 124°W, and (d) 34°W, which correspond to 0°, 90°E, 180°, and 90°W, respectively, in the ‘Claudia’ system (original coordinate system for Vesta). The illumination direction is shown with an orange circle on each of the hillshades. The hillshades are in south polar stereographic projection. <2-columns, color>

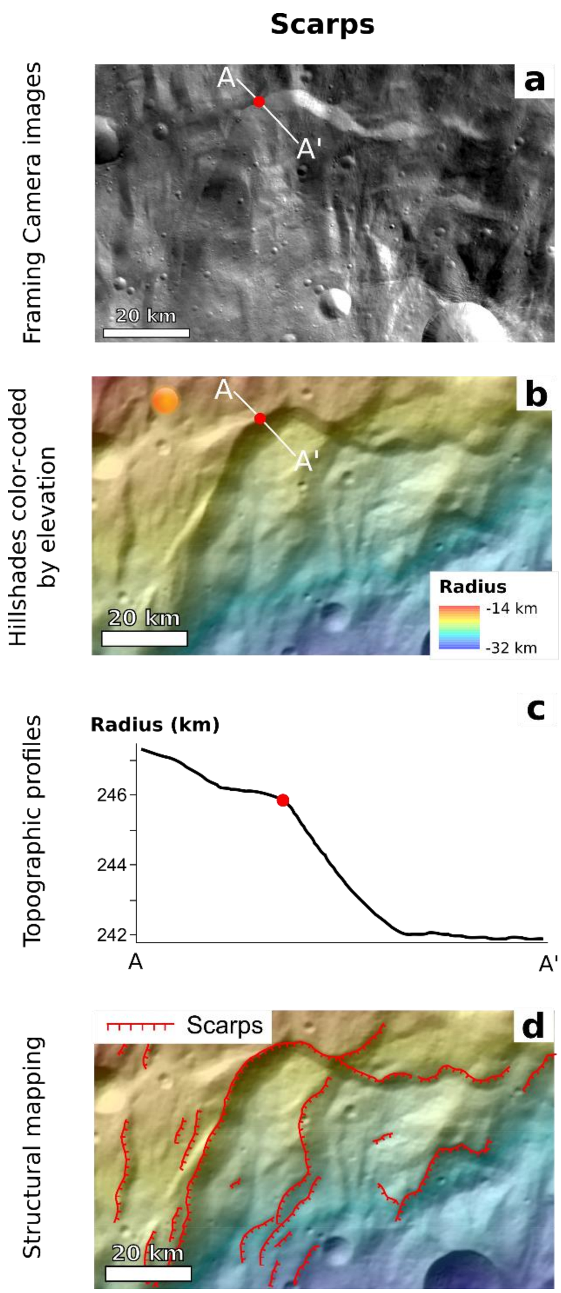

Figure 3. Identification and classification of scarps. (a) FC images and (b) hillshades shown color-coded by elevation. (c) Topographic profile A-A' across this scarp displays a sharp topographic break, marked by a red dot. The location of the profile is labeled in (a) and (b) with the point of the topographic break indicated as red dots. (d) Mapped scarp along the topographic break. All images are in south pole stereographic projection. The reference elevation is defined to be the mean planetary radius of 262 km. Refer to Figure 1 for the locations of this example.

<1-column, color>

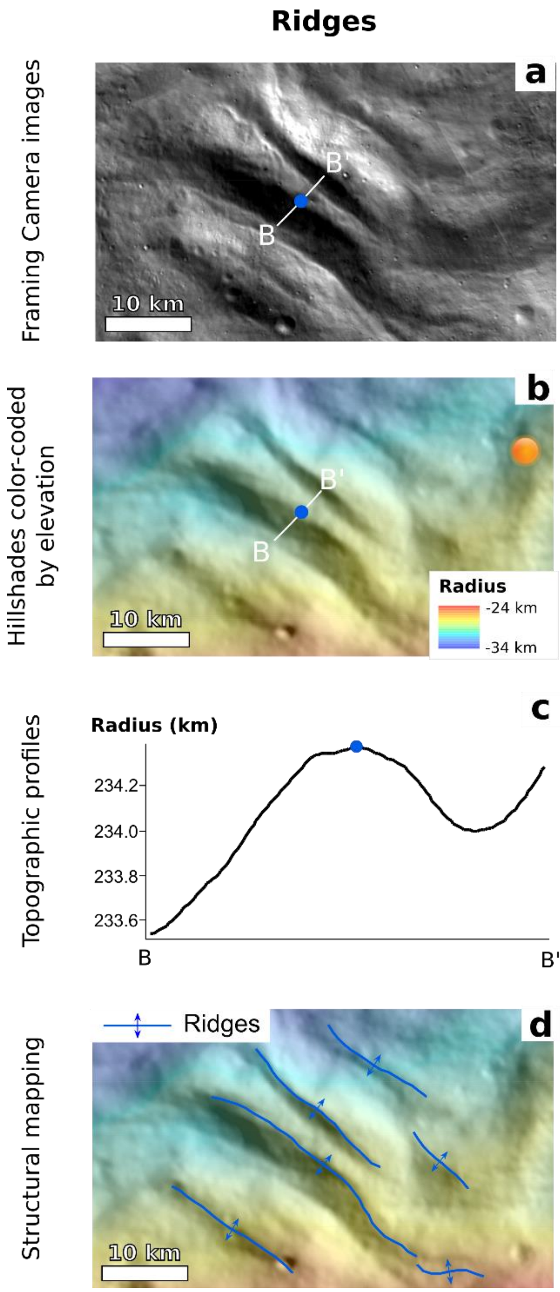

Figure 4. Identification and classification of ridges. (a) FC images and (b) hillshades shown color-coded by elevation. (c) Topographic profile B-B’ across this ridge displays positive relief with its crest marked by a blue dot. The location of the profile is labeled in (a) and (b) with the ridge crest also marked with blue dots. (d) Ridges are mapped on the hillshade by outlining their crests. Image details are the same as in Figure 3. <1-column, color>

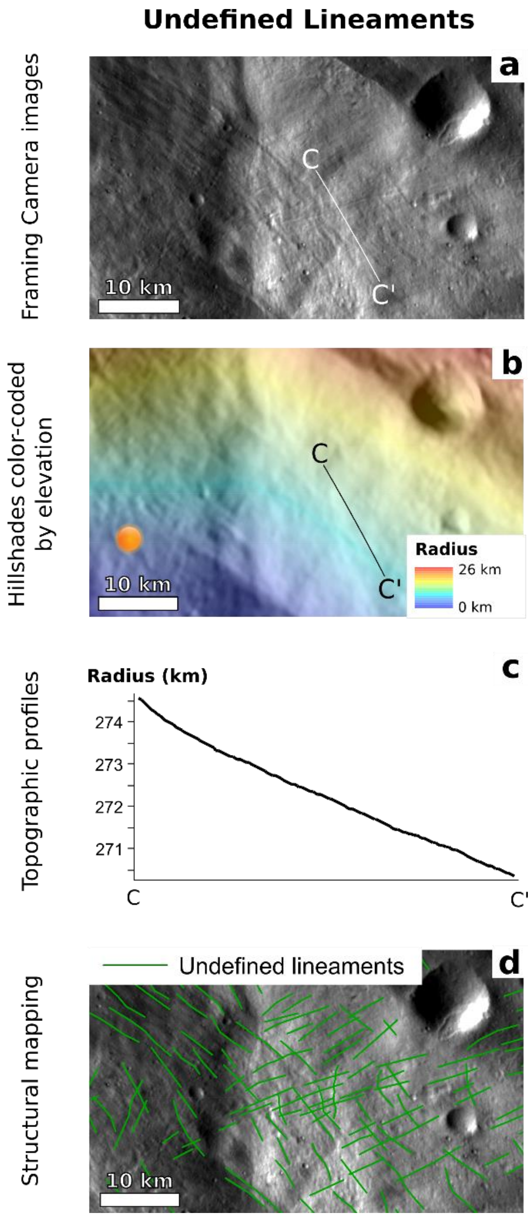

Figure 5. Identification and classification of undefined lineaments. (a) FC images and (b) hillshades shown color-coded by elevation. These lineaments are visible on the FC image in (a) but are barely recognizable or invisible on the hillshade in (b). (c) Topographic profile C-C’ displays no distinctive topographic properties of these lineaments. The location of the profile is

labeled in (a) and (b). (d) Undefined lineaments are mapped on the FC image. Image details are the same as in Figure 3. <1-column, color>

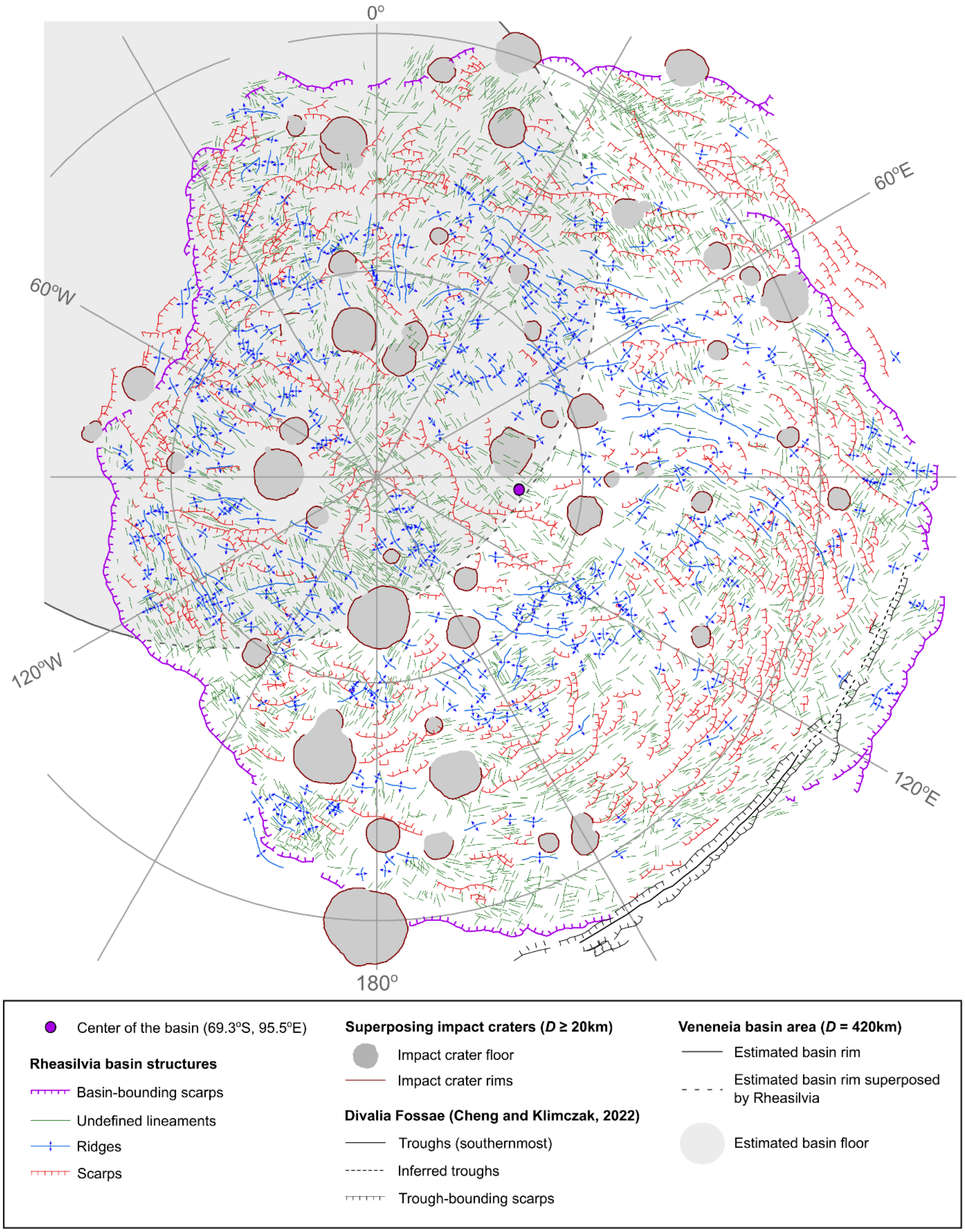
0°
60°E
60°W
120°W
120°E
180°
Center of the basin (69.3°S, 95.5°E)
Rheasilvia basin structures
Basin-bounding scarps
Undefined lineaments
Ridges
Scarps
Superposing impact craters (D ≥ 20km)
Impact crater floor
Impact crater rims
Divalia Fossae (Cheng and Klimczak, 2022)
Troughs (southernmost)
Inferred troughs
Trough-bounding scarps
Veneneia basin area (D = 420km)
Estimated basin rim
Estimated basin rim superposed by Rheasilvia
Estimated basin floor

Figure 6 Structural map of the Rheasilvia basin. The geometric mean center of the basin is calculated from the basin-bounding scarps and plotted as a purple dot. Refer to the text for the definition of structural map units. The map is in south polar stereographic projection. <2-columns>

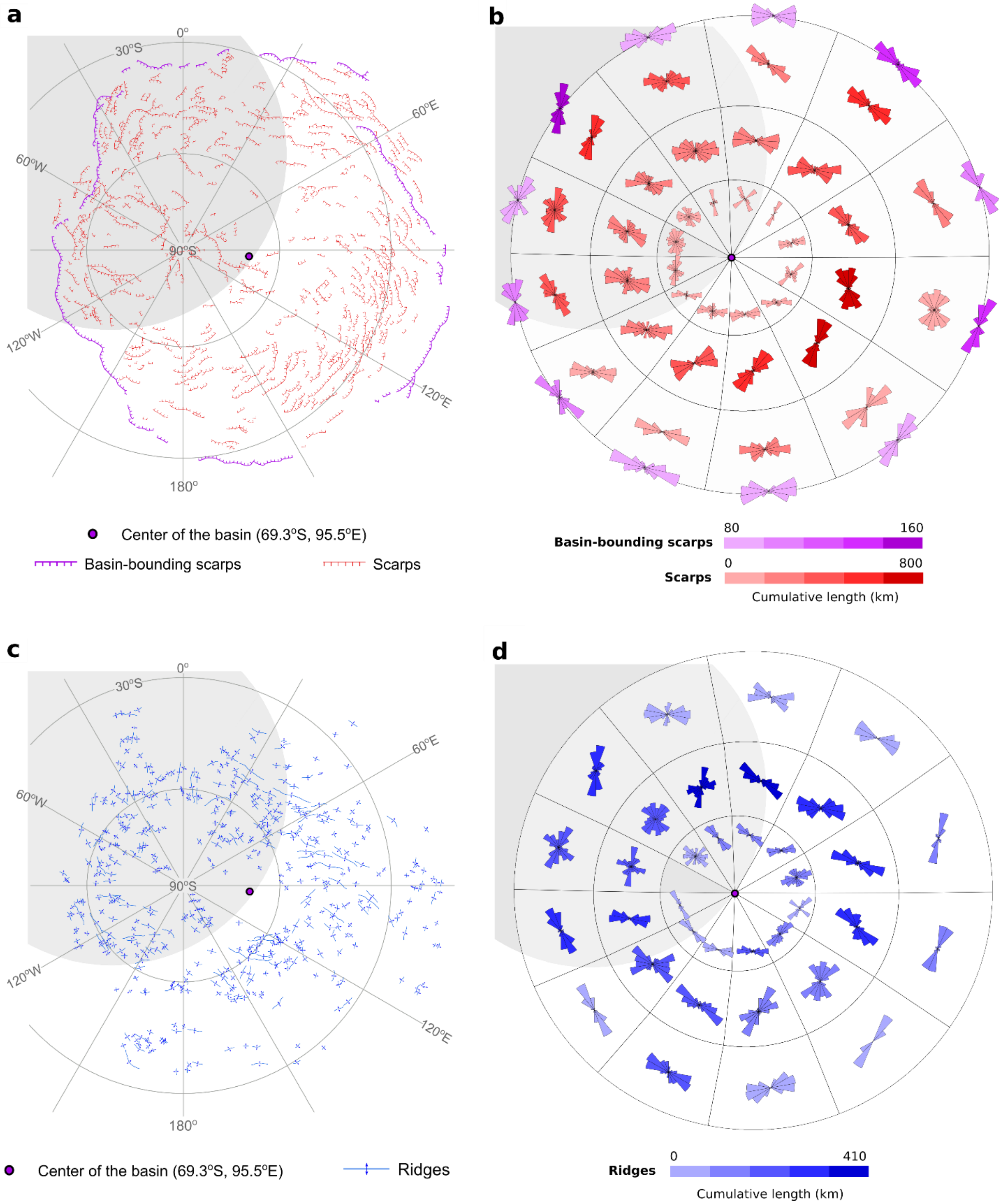
a
0°
30°S
60°E
60°W
90°S
120°W
120°E
180°
Center of the basin (69.3°S, 95.5°E)
Basin-bounding scarps
Scarps
b
Basin-bounding scarps
80
160
Scarps
0
800
Cumulative length (km)
c
0°
30°S
60°E
60°W
90°S
120°W
120°E
180°
Center of the basin (69.3°S, 95.5°E)
Ridges
d
Ridges
0
410
Cumulative length (km)

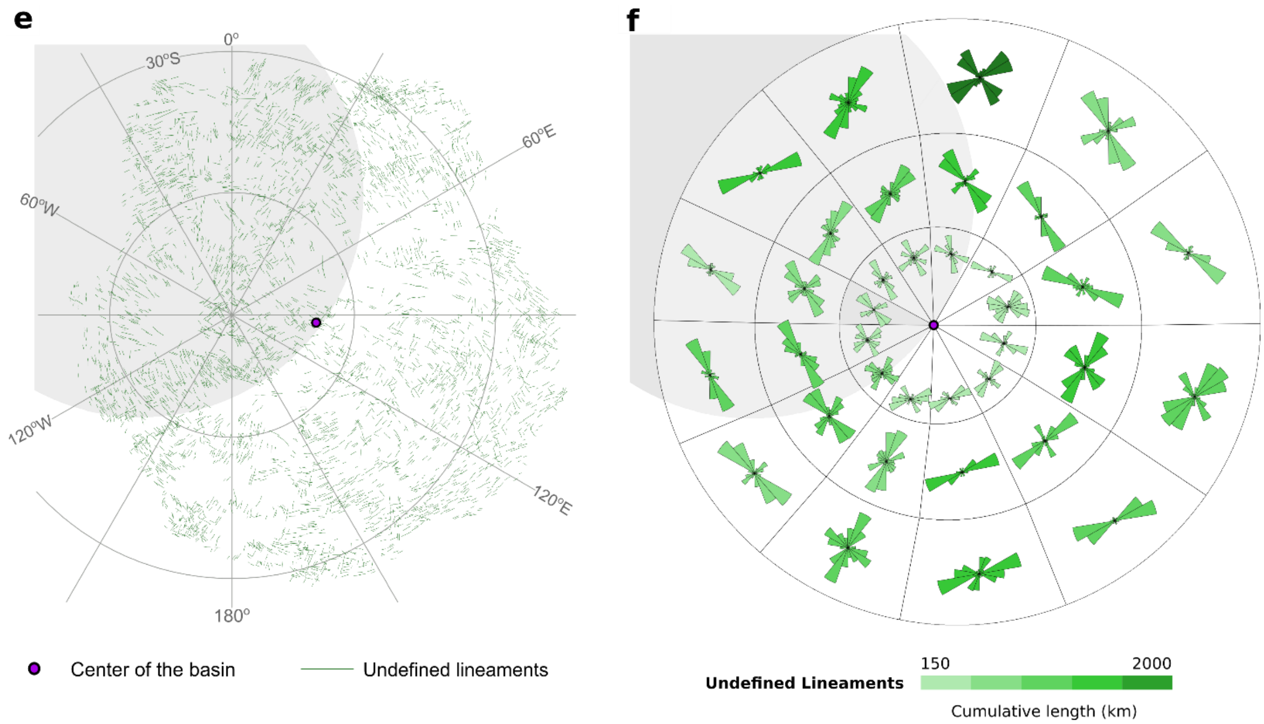

Figure 7 Structural units shown on separate maps on the left with their orientations presented as rose diagrams on the right. The basin was binned by three concentric circles with radii of 100 km, 200 km, and 300 km from the geometric mean center of the basin (purple dot) and further divided by 12 lines radiating from the center with an equal angle of 30°, resulting in 36 bins (outlined in black). As with previous maps (Figure 1 and 6), the estimated Veneneia basin floor is shaded in grey. (a) Basin-bounding scarps (purple) and scarps as they occur in the basin (red). (b) Length-weighted rose diagrams are plotted for each bin, with color variation showing their cumulative lengths for the basin-bounding scarps in purple and scarps within the basins in red. (c) Ridges (blue) as they occur on the map. (d) Length-weighted rose diagrams of ridges are plotted for each bin, with variations of intensity of the blue indicating their cumulative lengths. (e) Undefined lineaments (green) as they occur on the map. (f) Length-weighted rose diagrams of the undefined lineaments are plotted for each bin, with the intensity of the green color

indicating the cumulative lengths. All maps are in south polar stereographic projection. <2-column, color>

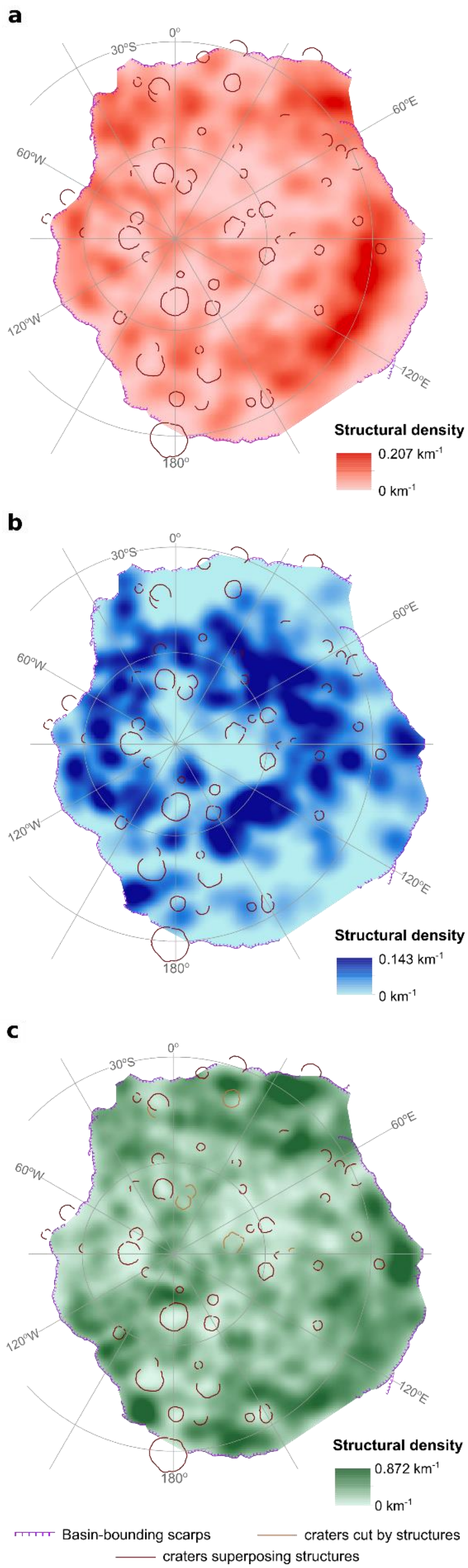
a
0°
30°S
60°E
60°W
120°W
120°E
180°
Structural density
0.207 km-1
0 km-1
b
0°
30°S
60°E
60°W
120°W
120°E
180°
Structural density
0.143 km-1
0 km-1
c
0°
30°S
60°E
60°W
120°W
120°E
180°
Structural density
0.872 km-1
0 km-1
Basin-bounding scarps
craters cut by structures
craters superposing structures

Figure 8 Structure density maps shown for (a) scarps in red, (b) ridges in blue, and (c) undefined lineaments in green across the Rheasilvia basin outlined by the basin-bounding scarps. Structural density is expressed in kilometers of structure length per square kilometers (km^{-1}) with darker colors representing a higher density across the basin. Rheasilvia basin-bounding scarps are shown in purple. The rims of post-Rheasilvia craters that superpose the structure type are outlined in dark brown, and those that are cut by the structure type are outlined in light brown. Note that all impact craters superpose scarps and ridges, whereas lineaments can be superposed by or cutting a crater. <1-column, color>

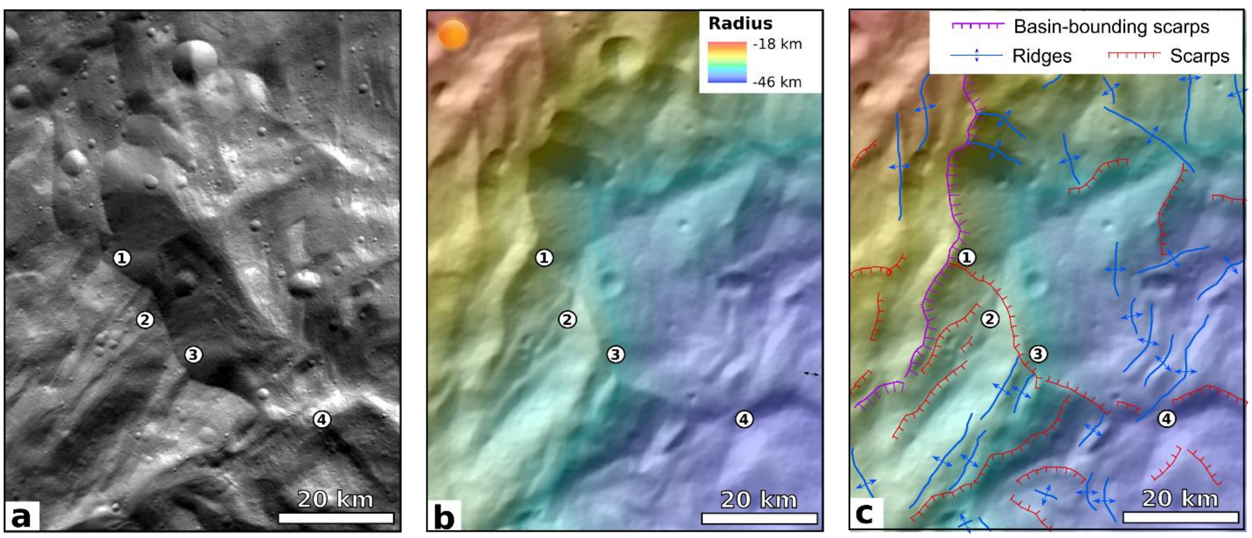

Figure 9. A representative area showing multiple examples of cross-cutting relationships between basin-bounding scarps, scarps within the basin, and ridges labeled by numbers. (a) FC image and (b) hillshade color-coded by elevation of an area displaying complex cross-cutting relationships of structures, including (1) a basin-bounding scarps cutting scarps within the basin, a large scarp cutting (2) smaller scarps and (3) ridges, and (4) a ridge cutting a scarp. No systematic cross-cutting relationships among the different structural units are observed across the

basin. The images are in south pole stereographic projection. The reference elevation is defined to be the mean planetary radius of 262 km. Refer to Figure 1 for the image location. <2-column, color>

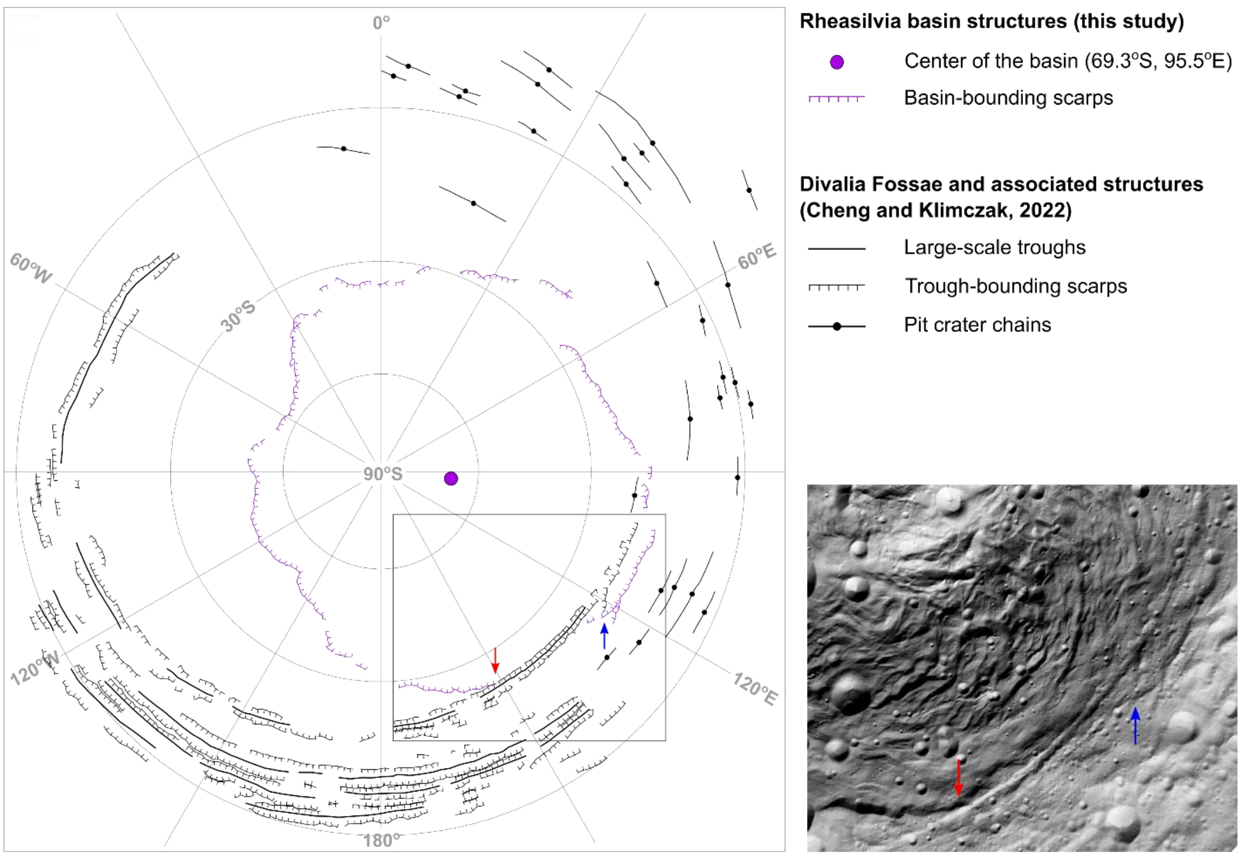

Figure 10. Structural map (left) and hillshade (right) showing the basin-bounding scarps of the Rheasilvia basin with Divalia Fossae mapped by Cheng and Klimczak (2022). The southernmost trough is cutting the basin-bounding scarps (marked with a red arrow) and lying within the basin (marked with blue arrows). The geometric mean center of the basin is plotted on the map with a purple dot to show its configuration with Divalia Fossae. Pit-crater chains associated with the troughs on Vesta are also shown on the structural map. The hillshade image (with the azimuth of 146°E from Figure 2b and its extent outlined in black lines on the structural map on the left)

captures the cross-cutting relationship of the southernmost trough of Divalia Fossa and the Rheasilvia basin-bounding scarps with the red and blue arrows. Refer to Figures 1 and 2 for the hillshade and elevation data. <2-column, color>

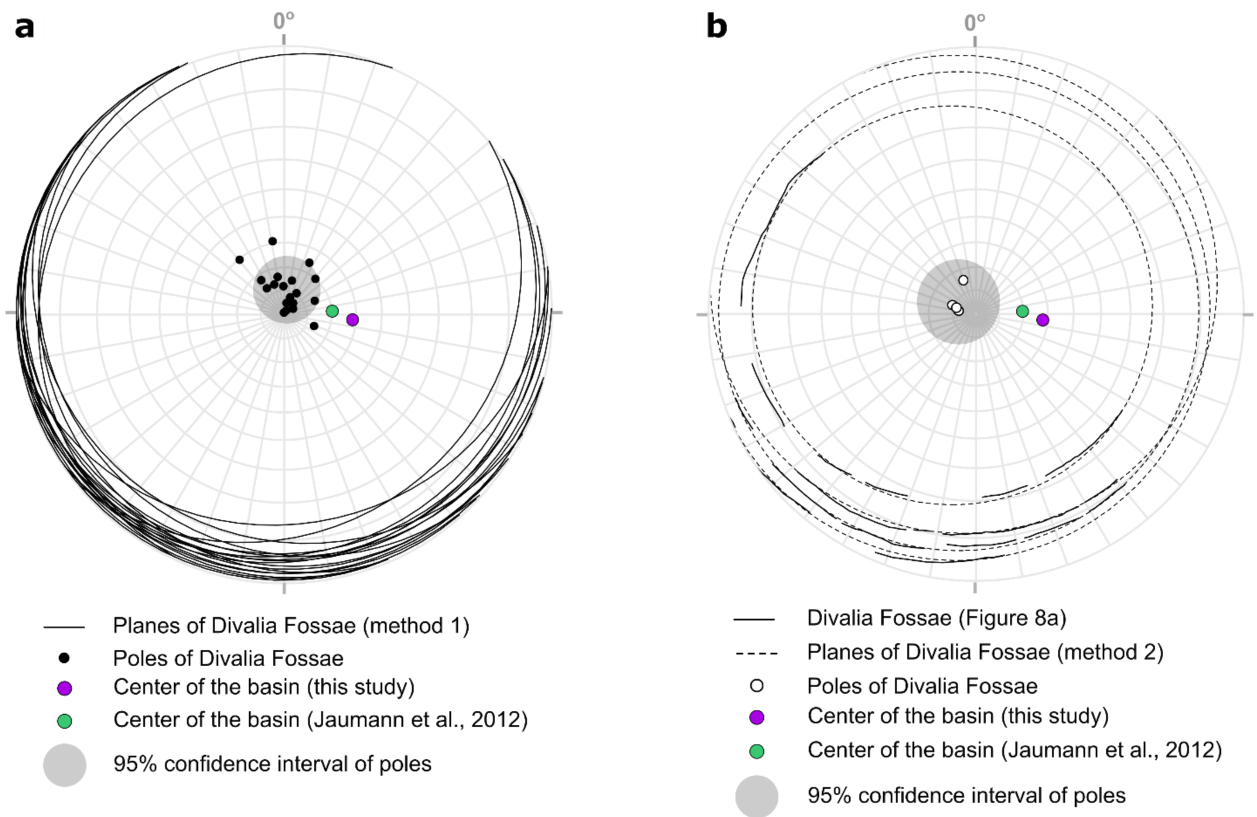

Figure 11. Equal area south pole projection stereonet showing the configuration of the Rheasilvia basin and Divalia Fossae. (a) The configuration of the Rheasilvia basin and Divalia Fossae is investigated using method 1 by Jaumann et al. (2012). Planes are defined by the center positions of the troughs segments mapped by Cheng and Klimczak (2022), represented by great circles shown in black. The center of the Rheasilvia basin calculated in this study and from Jaumann et al. (2012) are plotted as purple and green dots, respectively. The poles of the trough-defined planes are plotted in black. The 95% confidence ellipse of these poles is calculated and

highlighted in grey. (b) The configuration of the Rheasilvia basin and Divalia Fossae is investigated by defining small circles of the main trough structures (method 2). The 19 trough segments of Divalia Fossae (black lines) belong to four main structures (Cheng and Klimczak, 2022). The planes that best fit each of the four structures are presented as small circles in dashed lines with their poles shown as white dots. The 95% confidence ellipse of these poles is also shown in grey. The reader is advised that we applied the new coordinate system used for Vesta updated in 2014[2], which is different from the one used by Jaumann et al. (2012). <2-column, color>

[2] https://www.iau.org/news/announcements/detail/ann14003/